Transportation Science

Publication details, including instructions for authors and subscription information:
http://pubsonline.informs.org

Riemann Problem Resolution and Godunov Scheme for the Aw-Rascle-Zhang Model

Salim Mammar, Jean-Patrick Lebacque, Habib Haj Salem,

To cite this article:
Salim Mammar, Jean-Patrick Lebacque, Habib Haj Salem, (2009) Riemann Problem Resolution and Godunov Scheme for the Aw-Rascle-Zhang Model. Transportation Science 43(4):531-545. http://dx.doi.org/10.1287/trsc.1090.0283

TRANSPORTATION SCIENCE
Vol. 43, No. 4, November 2009, pp. 531–545
ISSN 0041-1655 | EISSN 1526-5447 | 09 | 4304 | 0531

informs

DOI 10.1287/trsc.1090.0283

Riemann Problem Resolution and Godunov Scheme for the Aw-Rascle-Zhang Model

Salim Mammar
Technical Department for Transport, Roads and Bridges (SETRA), F-92220 Bagneux, Cedex, France,
salim.mammar@developpement-durable.gouv.fr

Jean-Patrick Lebacque, Habib Haj Salem
INRETS/Gretia, "Les Descartes 2," F-93166 Noisy le Grand, Cedex, France
{lebacque@inrets.fr, haj-salem@inrets.fr}

Recently, Aw and Rascle and Zhang introduced a new second-order macroscopic model, following the theoretical investigations on the Payne-Whitham second-order modelling by Daganzo. The conserved variables in this model are the density and the relative flow. The aim of this paper is to solve the Riemann problem for the Aw-Rascle-Zhang (ARZ) model for all possible initial conditions, using an extended fundamental diagram. The resolution of the Riemann problem provides the user of the model with a set of nontrivial analytical solutions; it is also a prerequisite for the construction of numerical solution schemes. Some examples are given in which analytical solutions of the Riemann problem are discussed and compared to numerical solutions. The ARZ model shows better fit to real data than the embedded Lighthill-Whitham-Richards (LWR) model for the same set of physical parameters.

Key words: Riemann problem; analytical solutions; numerical solutions; shock waves; rarefaction waves; contact discontinuities; discretisation
History: Received: January 2007; revision received: November 2008; accepted: March 2009. Published online in *Articles in Advance* October 21, 2009.

1. Introduction

Second-order models were introduced by Payne (1971) and Witham (1974), to describe out-of-equilibrium traffic flow. The Payne-Whitham model exhibits some physical inconsistencies (the possibility of negative speed, for example) that were pointed out by Daganzo (1995). The past decade is fertile in terms of second-order dynamic traffic flow model developments aiming at overcoming the nonphysical solution. Among others, models were proposed by Del Castillo, Pintado, and Benitz (1993), Ross (1988), Aw and Rascle (2000), Zhang (1998, 2002), and Jiang, Wu, and Zhu (2002).

This paper is focused on the models proposed independently by Aw and Rascle (Aw and Rascle 2000) and Zhang (Zhang 2002), which are very similar. The two models are merged into the improved model, namely, "Aw, Rascle, and Zhang" (ARZ, for short). The ARZ model is a hyperbolic system of two conservation laws. The conserved variables are the density and the *relative flow*, i.e., the difference between the actual and the equilibrium flow, which is defined by the fundamental diagram, as in the Lighthill-Whitham-Richards (LWR) model (Lighthill and Whitham 1955; Richards 1956). In our previous paper (Lebacque et al. 2007a), it has been shown that the Riemann problem for the ARZ model admits solutions for all possible initial conditions only if the fundamental diagram is suitably extended. Based on this result, this paper presents the resolution of the hyperbolic system, which is a nontrivial task. The Riemann problem for the ARZ model for all initial conditions is presented, along with particular nontrivial solutions that are discussed according to the extension of the fundamental diagram hypothesis. Further, the resolution of the Riemann problem is the base of the construction of numerical schemes such as the Godunov scheme (Lebacque 1996; Kröner 1997).

The outline of this paper is as follows. First, the basic features of the ARZ model are recalled, and the waves of the model are analysed, under the assumption that the fundamental diagram has been suitably extended. The principles of the resolution of the Riemann problem for the ARZ model are introduced and solved analytically and numerically for three representative sets of initial conditions, showing the correctness of the numerical schemes. A comparison is made on a set of motorway data measurements, showing that the ARZ model recaptures traffic dynamics much better than the embedded LWR model for a fundamental diagram estimated on

the data scatter plot and the physical characteristics of the motorway.

2. The Description of the ARZ Model

In Lebacque et al. (2007a) the ARZ model is described. Let us recall the basic mathematical model equations:

1. Conservation equation:

$$\partial_t \rho(x,t) + \partial_x(\rho v)(x,t) = 0. \tag{1}$$

2. Momentum equation:

$$\partial_t v(x,t) + (v + \rho V_e'(\rho))(x,t)\partial_x v(x,t) = 0. \tag{2}$$

The meaning of the notations is as follows:

x, t:	the position and time;
∂_t, ∂_x:	the partial derivative with respect to time and space variables;
$\rho(x,t)$:	the density at time t and location x;
$v(x,t)$:	the speed at time t and location x;
$V_e(\rho, x)$:	the equilibrium speed (at location x).

To study the elementary waves associated with this model and to discuss the analytical solutions, it is necessary to rewrite this model in conservative form:

$$\begin{cases} \partial_t \rho(x,t) + \partial_x(\rho(x,t)v(x,t)) = 0, \\ \partial_t y(x,t) + \partial_x p(x,t) = 0, \end{cases} \tag{3}$$

with $I(x,t) \stackrel{\text{def}}{=} v(x,t) - V_e(\rho(x,t), x)$, the relative speed, i.e., the difference between the actual speed and the equilibrium speed; $y(x,t) \stackrel{\text{def}}{=} \rho(x,t)I(x,t) = q(x,t) - Q_e(\rho(x,t), x)$, the relative flow, i.e., the difference between the actual flow and the equilibrium flow (Figure 1); $Q_e(\rho, x)$, the equilibrium flow (at location x), i.e., the fundamental diagram; $q(x,t) \stackrel{\text{def}}{=} \rho(x,t)v(x,t)$, the flow at time t and location x; $p(x,t) \stackrel{\text{def}}{=} q(x,t)(v(x,t) - V_e(\rho(x,t), x)) = v(x,t)y(x,t)$, the relative pressure, i.e., the flux of relative flow; and $V_e(\rho, x)$, the equilibrium speed (at location x).

The fundamental diagram (Figure 1) is expressed by a piecewise quadratic relationship of flow as a function of density. This fundamental diagram will be used in subsequent analyses, as well as in applications.

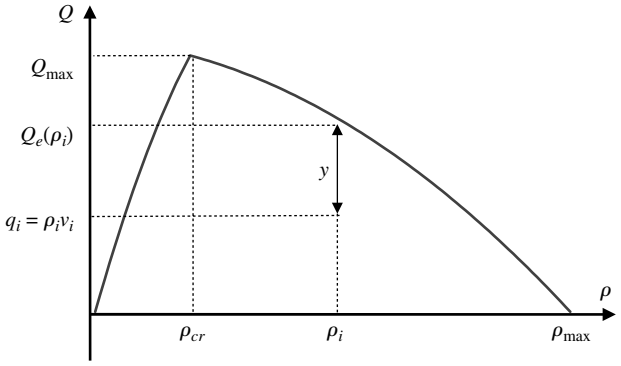

Figure 1 Physical Meaning of the y Variable

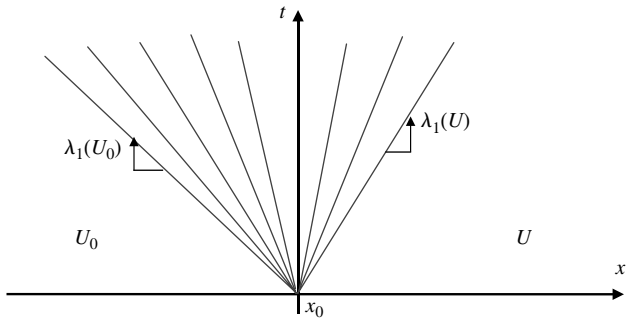

Figure 2 1-Rarefaction Wave

3. Mathematical Properties

In this section, we recall some basic mathematical properties of hyperbolic systems of conservation laws: concept of characteristic, Riemann invariant, and weak solution. For background material the reader is referred to Kröner (1997), Aw and Rascle (2000), Zhang (2002), and Lebacque, Mammar, and Haj-Salem (2007b).

3.1. Eigenvalues

The ARZ model (3) takes the form of a system of conservation laws:

$$\partial_t U + \partial_x F(U) = 0 \quad \text{with}$$

$$U = \begin{pmatrix} \rho \\ y \end{pmatrix}, \quad F(U) = \begin{pmatrix} y + \rho V_e(\rho) \\ \dfrac{y^2}{\rho} + y V_e(\rho) \end{pmatrix}, \tag{4}$$

where U denotes the vector of system state variables (the conserved variables) and $F(U)$ the flux vector.

Based on the computation of the gradient of flux vector: $A(U) \stackrel{\text{def}}{=} \nabla F(U)$, system (4) admits two distinct eigenvalues, $\lambda_1(U)$ and $\lambda_2(U)$, given by

$$\lambda_1(U) = \frac{y}{\rho} + V_e(\rho) + \rho V_e'(\rho) = v + \rho V_e'(\rho) \quad \text{and}$$
$$\lambda_2(U) = \frac{y}{\rho} + V_e(\rho) = v. \tag{5}$$

Consequently, system (4) is strictly hyperbolic for $\rho \neq 0$.

Equation (5) indicates that the largest eigenvalue is equal to flow speed v. As a consequence, the anisotropic character of traffic is strictly preserved.

The computation of the eigenvectors $r_1(U)$ and $r_2(U)$ associated to each eigenvalue yields

$$r_1(U) = \begin{pmatrix} -\rho \\ -y \end{pmatrix} \quad \text{and} \quad r_2(U) = \begin{pmatrix} 1 \\ v - Q_e'(\rho) \end{pmatrix}. \tag{6}$$

The eigenvalue $\lambda_1(U)$ is genuinely nonlinear (GNL) following

$$\nabla\lambda_1(U) \cdot r_1(U) = -\rho Q_e''(\rho) > 0, \tag{7}$$

which is positive, assuming that the equilibrium flow density relationship Q_e is concave. The waves associated to the first eigenvalue are either shock or rarefaction waves (Figure 2). The field $r_1(U)$ is defined in such a way that

$$\nabla\lambda_1(U)\cdot r_1(U) > 0$$

is said to be *normalized*, meaning that eigenvalue λ_1 increases in the direction of eigenvector r_1.

A traffic state U can be connected to a traffic state U_0 if and only if $I(U) = I(U_0)$ (with I the relative speed).

A similar calculation shows that eigenvalue $\lambda_2(U)$ is linearly degenerate because of the value of the following product (by definition):

$$\nabla\lambda_2(U)\cdot r_2(U) = 0. \tag{8}$$

As a consequence, the waves associated with the second eigenvalue correspond to the contact singularities.

A traffic state U can be connected to a traffic state U_0 if and only if $v(U) = v(U_0)$.

3.2. Rarefaction Waves

The rarefaction wave associated with the 1-wave is a function of the parameter $\xi = x/t$. Indeed, rarefaction waves are self-similar. If a rarefaction wave connects left state $U_0(x \le 0, t = 0)$ to right state $U(x \ge 0, t = 0)$, it follows that inside the wave:

$$\begin{cases} \lambda_1(U(\xi)) = \dfrac{x}{t} \overset{\text{def}}{=} \xi, \\ \det\left(\dfrac{d}{d\xi}U(\xi), r_1(\xi)\right) = 0. \end{cases} \tag{9}$$

(The information in the 1-wave propagates at speed $\lambda_1 = x/t$.) Equation (9) expresses that $U(\xi)$ is an integral line, parameterized by ξ, of the field $r_1(U)$ in the phase space.

Note that

$$I(U(\xi)) = I(U(\xi_0)) \quad \Leftrightarrow \quad v(\xi) - V_e(\rho(\xi)) = v_0 - V_e(\rho_0). \tag{10}$$

Moreover, eigenvalue λ_1 must satisfy the following condition:

$$\lambda_1 = v(\xi) + \rho(\xi)V_e'(\rho(\xi)) = \xi. \tag{11}$$

Combining Equations (10) and (11), the rarefaction wave is described by:

$$\begin{cases} \xi = \dfrac{x}{t} \ge v_0, \\ \rho(\xi) = Q_e'^{-1}(\xi - (v_0 - V_e(\rho_0))), \\ v(\xi) = V_e(\rho(\xi)) + v_0 - V_e(\rho_0). \end{cases} \tag{12}$$

It follows from (12) that in a rarefaction wave, $v(\xi)$ and $y(\xi)$ must be increasing functions, and $\rho(\xi)$ must be a decreasing function of parameter ξ, which represents the slope of the characteristics (the "rarefaction fan"). Thus, $\rho(\xi) \le \rho_0$ and $y(\xi) \ge y_0$.

3.3. 1-Shock Waves, Contact Discontinuities (2-Waves)

Let us consider two traffic states $U_l(\rho_l, y_l)$ and $U_r(\rho_r, y_r)$ located on the left and the right of discontinuity point x_0. A 1-shockwave or a 2-wave connecting traffic states $U_r(\rho_r, y_r)$ and $U_l(\rho_l, y_l)$ propagates at a speed s that satisfies the following relation (Rankine-Hugoniot conditions (Kröner 1997)):

$$F(U_r) - F(U_l) = s(U_r - U_l) \quad \Leftrightarrow \quad \det|F(U_r) - F(U_l), U_r - U_l| = 0. \tag{13}$$

The solutions of (13) are given by

$$v_r - v_l = 0 \quad \text{(2-contact discontinuity)}, \tag{14}$$

$$v_r - V_e(\rho_r) - (v_l - V_e(\rho_l)) = 0 \quad \text{(1-shock waves)}. \tag{15}$$

Equation (15) gives the integral line of 1-shock waves.

Figure 3 depicts the locuses, given a state of traffic U_l, of all traffic states U_r connected to U_l by a 1-shock, a 1-rarefaction wave, or a contact discontinuity (1- and 2-curves, i.e., integral lines of 1- and 2-field).

Two traffic states, U_l and U_r, connected by a 1-wave satisfy the relationship (15), and they are connected by a 1-rarefaction wave if $\rho_l > \rho_r$ and by a 1-shock if $\rho_l < \rho_r$. Because $v_r - v_l = V_e(\rho_r) - V_e(\rho_l)$ using (15) and V_e is a decreasing function, states U_l and U_r are connected by a rarefaction wave if $v_l < v_r$ (*traffic acceleration*) and by a 1-shock if $v_l > v_r$ (*traffic deceleration*).

Contact discontinuities (2-waves) propagate *discontinuities of the relative speed or flow*, but the speed itself is equal on both sides of the discontinuity, as expressed by (14).

3.4. Riemann Problem

The resolution of the Riemann problem consists in: defining piecewise constant initial conditions with a

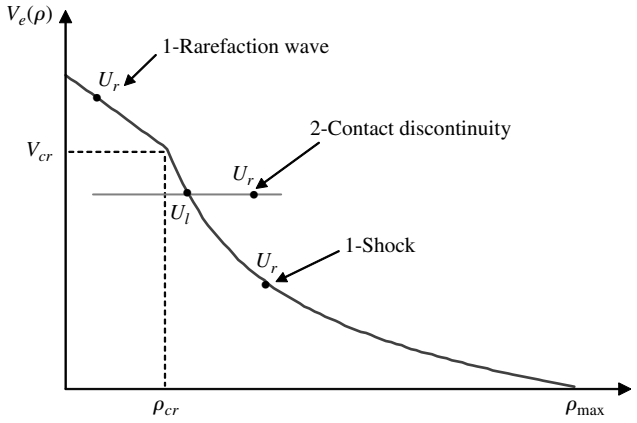

Figure 3 **1-Rarefaction Wave, 1-Shock, and 2-Contact Discontinuity in the (ρ, v) Plane**

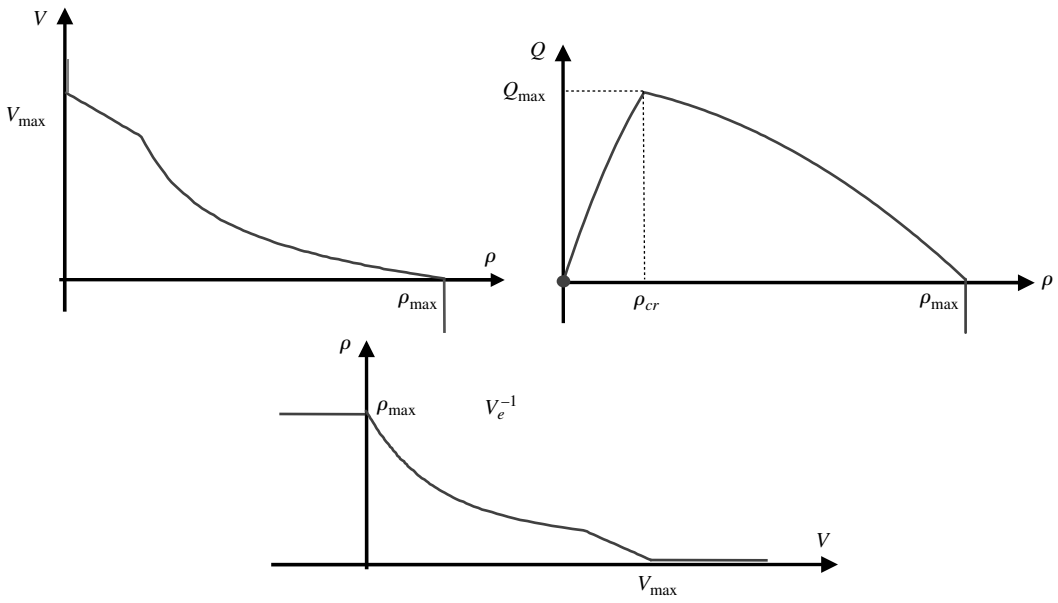

Figure 4 Extension of the Speed-Density Relationship

single discontinuity and finding self-similar solutions. The initial conditions are defined as follows:

$$\begin{cases} U(x,0) = U_l & \text{if } x < 0, \\ U(x,0) = U_r & \text{if } x > 0. \end{cases} \tag{16}$$

Following, for example, Kröner (1997), the general solution of the Riemann problem includes:

1. 1-wave connecting state U_l to an intermediate state U_0 to be calculated;
2. 2-wave connecting intermediate state U_0 to state U_r.

The main practical results of the resolution of the Riemann problem are v_w, q_w, p_w, and ρ_w: the speed, the flow, the pressure, and the density at the origin for $t > 0$, respectively.

The original ARZ model does not admit, in some cases, any solution to the Riemann problem. In Lebacque, Mammar, and Haj-Salem (2007a), it has been shown that the fundamental diagram should be prolonged as depicted in Figure 4, to solve the Riemann problem always. More intuitively, it is the inverse function V_e^{-1} that must be prolonged, as is shown by Figure 4, according to

$$\begin{aligned} V_e^{-1}(v) &= 0 \qquad \text{if } v \geq V_{\max}, \\ V_e^{-1}(v) &= \rho_{\max} \quad \text{if } v \leq 0. \end{aligned}$$

The function V_e^{-1} will be shown to be fundamental in the solution of the Riemann problem.

4. Discussions and Analysis of the General Solutions

Assume that U_l and U_r are the boundary conditions at the right and the left, respectively, of the intermediate state. The intermediate state U_0 is given by

$$v_0 = V_e(\rho_0) + (v_l - V_e(\rho_l)) \tag{17a}$$

$$\text{and} \quad v_0 = v_r. \tag{17b}$$

Equation (17a) expresses the 1-wave condition between states U_l and U_0; (17b) the 2-wave condition between U_0 and U_l. The general solution of the system Equations (17a) and (17b) is given by

$$\begin{cases} v_0 = v_r, \\ \rho_0 = V_e^{-1}(v_r - v_l + V_e(\rho_l)). \end{cases} \tag{18}$$

By taking into account the extension of the speed-density relationship reported in Figure 4, it is necessary to handle the argument of function V_e^{-1}, which is equal to $v_r - v_l + V_e(\rho_l)$. Depending on how this argument compares with 0 and $V_{\max}$, three cases can be distinguished and will be discussed in the following subsections.

4.1. Case 1: $v_r - v_l + V_e(\rho_l) > V_{\max}$

In this case we assume that the argument of V_e^{-1}: $v_r - v_l + V_e(\rho_l) > V_{\max}$; thus, it follows that $\rho_0 = 0$ and $v_0 = v_r$. On the other hand, $v_r - v_l > 0$. Thus, the Riemann problem solutions are:

1. rarefaction wave (RW) connecting $U_l \to U_0$; and
2. contact discontinuity (CD) connecting $U_0 \to U_r$.

The rarefaction wave (RW) connecting $U_l \to U_0$ itself must be decomposed into two parts:

1. rarefaction wave (RW-1) connecting $U_l \to U_*$, with U_* defined by $\rho_* = 0$ and $v_* = V_{\max} + v_l - V_e(\rho_l)$; and
2. rarefaction wave (RW-2) connecting $U_* \to U_0$ with $\rho = 0$ and the speed and wave speed equal and increasing from $V_{\max} - v_l + V_e(\rho_l)$ to v_r.

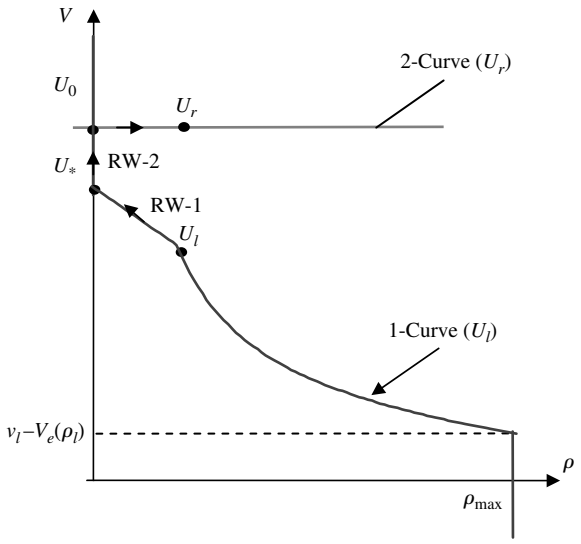

Figure 5 **Solution of the Riemann Problem in the Plane** (ρ, v)

The speed of the characteristics in 1-rarefaction waves is equal to

$$\lambda_1 = v + \rho V_e'(\rho) = Q_e'(\rho) + v_l - V_e(\rho_l)$$

because in a 1-rarefaction wave, $v = V_e(\rho) + (v_l - V_e(\rho_l))$, with Q_e' the derivative with respect to the density of the equilibrium flow.

Concerning the (RW-1) wave connecting $U_l \to U_*$, the Riemann problem solution can be expressed using the $\xi = x/t$ definition as follows (refer to formula (12)):

$$\begin{cases} \lambda_1 = \xi = \dfrac{x}{t}, \\ \rho(\xi) = Q_e'^{-1}(\xi - v_l + V_e(\rho_l)), \\ v(\xi) = V_e(\rho(\xi)) + v_l - V_e(\rho_l). \end{cases} \tag{19}$$

System (19) can be written also as

$$\begin{cases} \lambda_1 = \xi = Q_e'(\rho) + v_l - V_e(\rho_l), \\ v = V_e(\rho) + v_l - V_e(\rho_l). \end{cases} \tag{20}$$

Systems (19) and (20) are equivalent. However, the differences concern the use of the solution parameters (ξ) and ρ, respectively. Both parameters are useful. In particular, system (19) is used for computation of the limits of the rarefaction wave, whereas system (20) is used for traffic volume and pressure calculation at the origin $(\xi = 0)$.

The characteristic that bounds the (RW-1) wave on the left carries density ρ_l, and its speed reads as

$$\lambda_1 = Q_e'(\rho) + v_l - V_e(\rho_l) \;\Rightarrow\; \lambda_{1,l} = v_l + \rho_l V_e'(\rho_l). \tag{21}$$

The characteristic of state U_* that separates the (RW-1) and (RW-2) waves carries density $\rho = 0$, and its speed reads as

$$\lambda_{1,*} = V_{\max} + v_l - V_e(\rho_l). \tag{22}$$

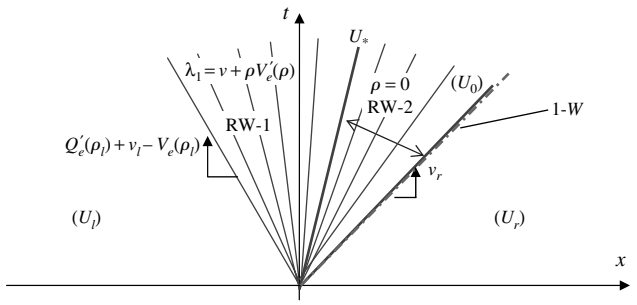

Figure 6 **Characteristics in** (x, t) **Plane of RW and CD Waves**

The (RW-2) characteristics comprised between U_* characteristic with speed $V_{\max} - v_l - V_e(\rho_l)$ and U_0 characteristic with speed v_r (see Figure 5) carry density $\rho = 0$. Their speed increases from $V_{\max} - v_l - V_e(\rho_l)$ to v_r. Figure 6 depicts in plane (x, t) the different characteristics of all cases.

By construction, we can note that $\lambda_{1,*} \geq v_l \geq 0$.

Consequently, in this case, two subcases can be distinguished according to the sign of $\lambda_{1,l}$ for the computation at the origin $(\xi = 0)$ of the flow (q), the pressure (p), and the density. Let us recall that v_w, q_w, p_w, and ρ_w are, respectively, the speed, the flow, the pressure, and the density to be calculated at the origin.

Case 1.1. $\lambda_l = v_l + \rho_l V_e'(\rho_l) \leq 0$. In this case $\lambda_{1,w} = 0$ because $\lambda_{1,*} \geq v_l \geq 0$ (state U_* on the right hand of the origin). Following (18) the density is given by

$$\rho_w = Q_e'^{-1}(-v_l + V_e(\rho_l)). \tag{23}$$

Speed v_w given by Equation (19) reads as

$$v_w = V_e(\rho_w) + v_l - V_e(\rho_l). \tag{24}$$

Finally, the Riemann problem solutions read as

$$\begin{cases} v_w = V_e(\rho_w) + v_l - V_e(\rho_l), \\ \rho_w = Q_e'^{-1}(-v_l + V_e(\rho_l)), \\ q_w = \rho_w v_w, \\ p_w = \rho_w v_w (v_w - V_e(\rho_w)) = q_w(v_l - V_e(\rho_l)). \end{cases} \tag{25}$$

Case 1.2. $\lambda_l = v_l + \rho_l V_e'(\rho_l) \geq 0$. The traffic state at the origin $(\xi = 0)$ is U_l. Thus, the solution of Riemann's problem is given by

$$\begin{cases} v_w = v_l, \\ \rho_w = \rho_l, \\ q_w = q_l = \rho_l v_l, \\ p_w = p_l = q_l(v_l - V_e(\rho_l)). \end{cases} \tag{26}$$

4.2. Case 2: $0 \leq v_r - v_l + V_e(\rho_l) \leq V_{\max}$

In this case, we assume that the argument of V_e^{-1}: $0 \leq v_r - v_l + V_e(\rho_l) \leq V_{\max}$. Two subcases can be distinguished according to values v_l and v_r:

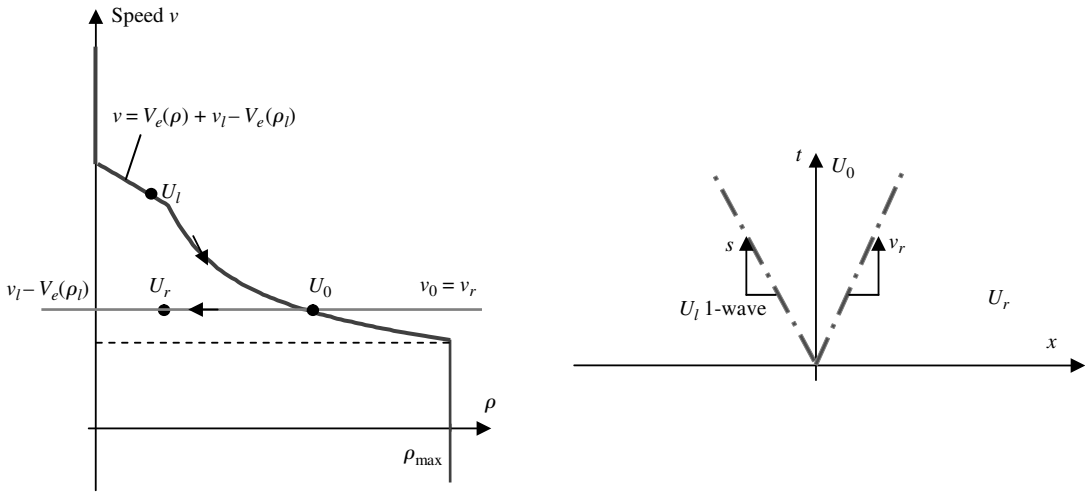

Figure 7 **Traffic States in Plane v, Characteristics in (x, t) Plane of SW and CD Waves**

Case 2.1. $v_r \le v_l$. Thus, the Riemann problem solutions are:

1. 1-shock wave (SW) connecting $U_l \to U_0$; and
2. 2-contact discontinuity (CD) connecting $U_0 \to U_r$.

Intermediate state U_0 is given by Equation (18). The shock wave propagation speed can be evaluated using the Rankine-Hugoniot relation as follows:

$$s = \frac{q_0 - q_l}{\rho_0 - \rho_l} \;\Rightarrow\; v_r - s = \rho_l \frac{v_l - v_r}{\rho_0 - \rho_l} > 0 \tag{27}$$

because $\rho_0 > \rho_l$, $v_l > v_r$.

To compute the intermediate state defined by v_w and ρ_w, we can distinguish both subcases according to the sign of s:

Case 2.1.1. $q_0 - q_l \le 0$ $(s \le 0)$. The solution of the Riemann problem is given by

$$\begin{cases} v_w = v_0 = v_r, \\ \rho_w = \rho_0 = V_e^{-1}(v_r - v_l + V_e(\rho_l)), \\ q_w = q_0 = \rho_0 v_r, \\ p_w = q_w(v_l - V_e(\rho_l)). \end{cases} \tag{28}$$

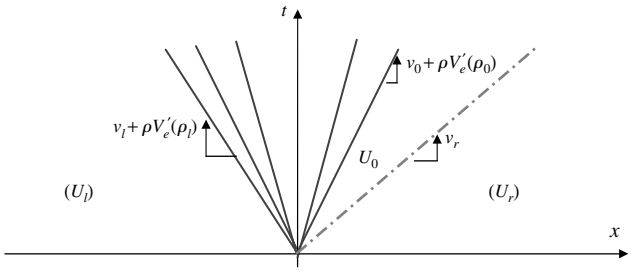

Figure 8 **Case 2.2.**

Case 2.1.2. $q_0 - q_l \ge 0$ $(s \ge 0)$. The solution of the Riemann problem is given by

$$\begin{cases} v_w = v_l, \\ \rho_w = \rho_l, \\ q_w = q_l = \rho_l v_l, \\ p_w = p_l = q_l(v_l - V_e(\rho_l)). \end{cases} \tag{29}$$

Note that for these two cases, $q_w = \mathrm{Min}(q_l, q_0)$.

Case 2.2. $v_r \ge v_l$ (Figure 8). In this case, the Riemann problem solutions are as follows:

1. rarefaction wave (RW) connecting $U_l \to U_0$; and
2. contact discontinuity (CD) connecting $U_0 \to U_r$.

The speed of the characteristic that carries U_0 is given by $\lambda_1 = v_0 + \rho_0 V_e'(\rho_0)$, with

$$\begin{cases} v_0 = v_r, \\ \rho_0 = V_e^{-1}(v_r - v_l + V_e(\rho_l)). \end{cases}$$

Three cases must be analysed: $\lambda_1(U_l) \ge 0$ and $(U_w = U_l)$; $\lambda_1(U_0) \le 0$ and $(U_w = U_0)$; and $\lambda_1(U_l) \le 0 \le \lambda_1(U_0)$.

Case 2.2.1. $\lambda_1(U_l) = v_l + \rho_l V_e'(\rho_l) \ge 0$. In this case, the Riemann problem solutions are

$$\begin{cases} v_w = v_l, \\ \rho_w = \rho_l, \\ q_w = q_l = \rho_l v_l, \\ p_w = p_l = q_l(v_l - V_e(\rho_l)). \end{cases} \tag{30}$$

Case 2.2.2. $\lambda_1(U_0) = v_0 + \rho_0 V_e'(\rho_0) \le 0$. In this case, the Riemann problem solutions are

$$\begin{cases} v_w = v_r, \\ \rho_w = \rho_0 = V_e^{-1}(v_r - v_l + V_e(\rho_l)), \\ q_w = \rho_w v_w, \\ p_w = q_w(v_l - V_e(\rho_l)). \end{cases} \tag{31}$$

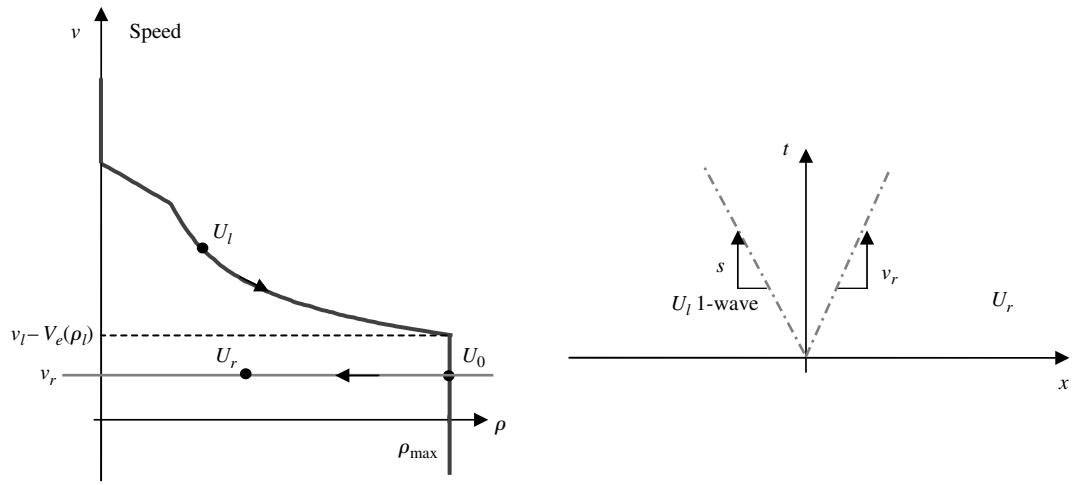

Figure 9 Case 3

Case 2.2.3. $\lambda_1(U_l) = v_l + \rho_l V_e'(\rho_l) \le 0 \le \lambda_1(U_0) = v_0 + \rho_0 V_e'(\rho_0)$. In this case, the Riemann problem solutions are similar to those in Equation (26), Case 1.2:

$$\begin{cases} v_w = V_e(\rho_w) + v_l - V_e(\rho_l), \\ \rho_w = Q_e'^{-1}(-v_l + V_e(\rho_l)), \\ q_w = \rho_w v_w, \\ p_w = q_w(v_l - V_e(\rho_l)). \end{cases} \tag{32}$$

4.3. Case 3: $v_r \le v_l - V_e(\rho_l)$

In this case, we assume that the argument of V_e^{-1} is negative: $v_r - v_l + V_e(\rho_l) \le 0$, and the intermediate state is characterised by density $\rho_0 = \rho_{\max}$ and speed $v_0 = v_r$. In real life, such nonzero speeds at maximum density will be very small. Consequently, the following waves can precede the contact discontinuity (CD) $U_0 \to U_r$:

1. $v_r \le v_l$: shock wave (SW) connecting $U_l \to U_0$; and
2. $v_r \ge v_l$: rarefaction wave (RW) connecting $U_l \to U_0$.

However, condition $v_r \ge v_l$ is incompatible with condition $v_r - v_l + V_e(\rho_l) \le 0$. As a matter of fact, the two conditions together imply the inequality:

$$0 \le v_r - v_l \le -V_e(\rho_l) \quad \text{(contradiction)}.$$

The speed of the shock waves is given by

$$\begin{aligned} s = \frac{\rho_{\max} v_r - \rho_l v_l}{\rho_{\max} - \rho_l} \quad &\Rightarrow \quad s - v_r \\ = \rho_l \frac{v_r - v_l}{\rho_{\max} - \rho_l} < 0; \quad &\text{thus } s < v_r. \end{aligned}$$

We can observe that $s \ge 0 \Rightarrow v_r \ge (\rho_l/\rho_{\max}) v_l$, which corresponds to subcase 2.1, which has been analyzed previously:

Case 3.1. $v_r \ge (\rho_l/\rho_{\max}) v_l$. In this case, the Riemann problem solution reads as

$$\begin{cases} v_w = v_l, \\ \rho_w = \rho_l, \\ q_w = q_l = \rho_l v_l, \\ p_w = p_l = q_l(v_l - V_e(\rho_l)). \end{cases} \tag{33}$$

Case 3.2. $v_r \le (\rho_l/\rho_{\max}) v_l$. In this case, the Riemann problem solutions are

$$\begin{cases} v_w = v_0 = v_r, \\ \rho_w = \rho_0 = \rho_{\max}, \\ q_w = q_0 = \rho_{\max} v_r, \\ p_w = q_w(v_l - V_e(\rho_l)). \end{cases} \tag{34}$$

Note that, as for Case 2.1,

$$q_w = \text{Min}(q_l, q_0),$$

which is natural because $s \le 0 \Leftrightarrow q_0 \le q_l$.

Summary

The expressions derived in this section, namely, Equations (25) to (34), express the fluxes at the origin as a function of the initial data, that is, they define the fluxes at the origin as function **F** of the initial data:

$$\text{(38) to (47)} \quad \Leftrightarrow \quad \begin{pmatrix} q_w \\ p_w \end{pmatrix} \stackrel{\text{def}}{=} \mathbf{F}\left(\begin{pmatrix} \rho_l \\ y_l \end{pmatrix}, \begin{pmatrix} \rho_r \\ y_r \end{pmatrix} \right). \tag{35}$$

Note that in all cases, including (47), the relationship $p_w = q_w(v_l - V_e(\rho_l))$ holds (if the prolongation of the fundamental diagram is taken into account). This relationship will be analyzed in Lebacque, Mammar, and Haj-Salem (2007b).

5. Comparison of Analytical and Numerical Riemann Problem Solutions

To verify the obtained analytical solutions and the numerical solutions, three representative cases are selected and compared. The numerical solutions correspond to the discretization of the analytical solutions using the Godunov (Kröner 1997) numerical scheme.

The Godunov scheme, as applied to traffic modelling on a homogeneous motorway section, is based on the following ideas:

- The section is divided into cells $(c) = [x_{c-1}, x_c]$, time is divided into time steps $(t) = [t\Delta t, (t+1)\Delta t]$, with time-step interval Δt.
- Density ρ and relative flow y are assumed homogeneous on each cell (c) at the beginning of each time step (t), and they are equal to ρ_c^t and y_c^t, respectively. Thus, the density $\rho(x,t)$ and relative flow $y(x,t)$ are approximated at the beginning of each time step by piecewise constant function $\tilde{\rho}(x,t)$, $\tilde{y}(x,t)$:

$$\tilde{\rho}(x, t\Delta t) \stackrel{\text{def}}{=} \rho_c^t \quad \text{if } x \in (c) = [x_{c-1}, x_c],$$
$$\tilde{y}(x, t\Delta t) \stackrel{\text{def}}{=} y_c^t \quad \text{if } x \in (c) = [x_{c-1}, x_c].$$

- Flux between cells during a time step (t) is calculated by solving a Riemann problem at each cell boundary point x_c between cells (c) and $(c+1)$. The Courant-Friederich-Lewy (CFL) condition for any cell $(c) = [x_{c-1}, x_c]$ ensures that the solution of the Riemann problem at point x_{c-1} does not interact with the solution of the Riemann problem at point x_c. Thus, the flux vector is given by

$$\begin{pmatrix} q_c^t \\ p_c^t \end{pmatrix} = \mathbf{F}\left(\begin{pmatrix} \rho_c^t \\ y_c^t \end{pmatrix}, \begin{pmatrix} \rho_{c+1}^t \\ y_{c+1}^t \end{pmatrix}\right); \tag{36}$$

the outflow q_c^t of a cell will also be bounded by the residual storage capacity of the downstream cell $q_c^t \Delta t \le \Delta x_c(\rho_{\max,\,c+1} - \rho_{c+1}^t)$.

- The CFL condition is obtained by checking that the fastest wave emitted from point x_{c-1} (a 2-wave) does not intersect the slowest wave emitted from point x_c (a 1-wave, or the standing wave associated with the discontinuity of the fundamental diagram at point x_c). It follows by straightforward calculation that

$$\Delta t \le \frac{\Delta x_c}{V_{\max} + \text{Max}(W_{\max}, I_+)},$$

with I_+ the upper bound of $|I|$ in the input traffic data (measurements and initial conditions) and with $-W_{\max} \stackrel{\text{def}}{=} Q_e'(\rho_{\max})$. More precisely, the above CFL condition loses its validity for densities very close to jam density, for which the wave velocity can be arbitrarily large with the diagram of Figure 4. The density errors resulting from this approximation are small because of the constraint on cell outflows.

- Function **F** in expression (36) is the function giving the fluxes at the origin as a function of the initial conditions on the left- and right-hand sides, respectively, in the Riemann problem.
- The solution for the Riemann problem at each cell point x_c yields the approximate solution $\tilde{\rho}(x,\tau)$, $\tilde{y}(x,\tau)$ for any time $\tau \in (t) = [t\Delta t, (t+1)\Delta t]$.
- The averages of $\tilde{\rho}(x,(t+1)\Delta t)$ and $\tilde{y}(x,(t+1)\Delta t)$ over each cell yield the values at the beginning of time step $(t+1)$ of the cell means ρ_c^{t+1}, y_c^{t+1}; this is an orthogonal projection in the $\mathbf{L}^2$ sense of the approximate solution $\tilde{\rho}(x,(t+1)\Delta t)$, $\tilde{y}(x,(t+1)\Delta t)$ on the space of piecewise constant functions.
- The cell averages at time $(t+1)\Delta t$ can be calculated by applying the conservation of ρ and y during time step $(t+1)$ in each cell (c):

$$\begin{aligned} \rho_c^{t+1} &= \rho_c^t + \frac{\Delta t}{x_c - x_{c-1}}(-q_c^t + q_{c-1}^t), \\ y_c^{t+1} &= y_c^t + \frac{\Delta t}{x_c - x_{c-1}}(-p_c^t + p_{c-1}^t). \end{aligned} \tag{37}$$

For validation purposes of the numerical scheme, comparative studies between analytical and numerical solutions are performed. The considered fundamental diagram $Q_e(\rho)$ is depicted in Figure 10. It consists of two parabolic forms defined by the following relationship between traffic volume and density:

$$Q_e(\rho) = \rho\left[V_{\max} - \frac{\rho}{\rho_{cr}}(V_{\max} - V_{cr})\right] \quad \text{if } 0 \le \rho \le \rho_{cr},$$
$$Q_e(\rho) = W_{\max}(\rho_{\max} - \rho) + \alpha(\rho_{\max} - \rho)^2 \quad \text{if } \rho_{cr} \le \rho \le \rho_{\max},$$
$$\text{with } \alpha = (Q_{\max}/(\rho_{\max} - \rho_{cr})^2) - (W_{\max}/(\rho_{\max} - \rho_{cr})).$$

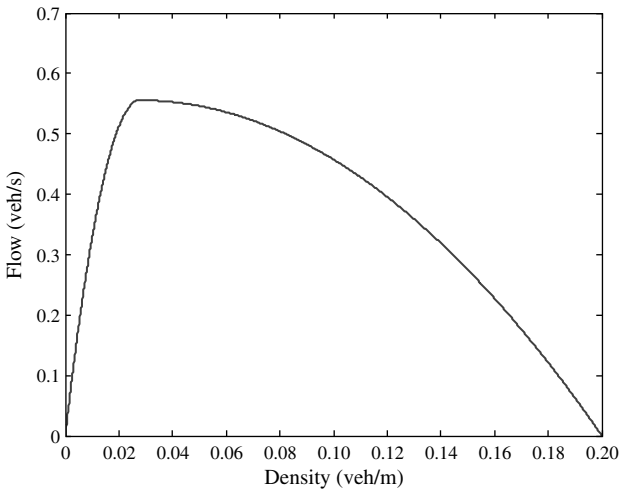

Figure 10 Fundamental Diagram

In this figure the following parameters are considered:

$$Q_e(\rho) \quad (\rho_{\max} = 0.2 \text{ veh/m}, \rho_{cr} = 0.0278 \text{ veh/m},$$
$$V_{cr} = 20 \text{ m.s}^{-1}, V_{\max} = 40 \text{ m.s}^{-1}, W_{\max} = 5 \text{ m.s}^{-1}).$$

By considering the definition of the relative traffic flow rate (y) and, according to the initial traffic conditions, three cases can be distinguished:

Case 1. The initial speed is given by the equilibrium speed ($y = \rho(v - V_e(\rho)) = 0$).

Case 2. The initial speed is lower than the equilibrium initial speed ($y = \rho(v - V_e(\rho)) < 0$).

Case 3. The initial speed is higher than the equilibrium speed ($y = \rho(v - V_e(\rho)) > 0$).

Let us analyse the solution of each case.

Case 1. ($y = \rho(v - V_e(\rho)) = 0$). Assume that the initial conditions are

$$U_l = (\rho_l = \rho_{cr}/2, v_l = V_e(\rho_{cr}/2)) \quad \text{and}$$
$$U_r = (\rho_{\max}, v_r = V_e(\rho_{\max}) = 0 \text{ m.s}^{-1}).$$

This case can be identified as Case 2.1.1 of the Riemann problem, previously described in §4.

For the numerical scheme, the time slice is chosen equal to $\Delta t = 2$ seconds and the segment length is equal to $\Delta x = 100$ meters.

In Figure 11, both solutions are reported at time $t = 40$ seconds. In particular, we can observe that the analytical and numerical solutions are very close.

To demonstrate the stability of the numerical scheme, another test is conducted with a modification of the time slice. As depicted in Figure 12, we can observe that both solutions are even more similar.

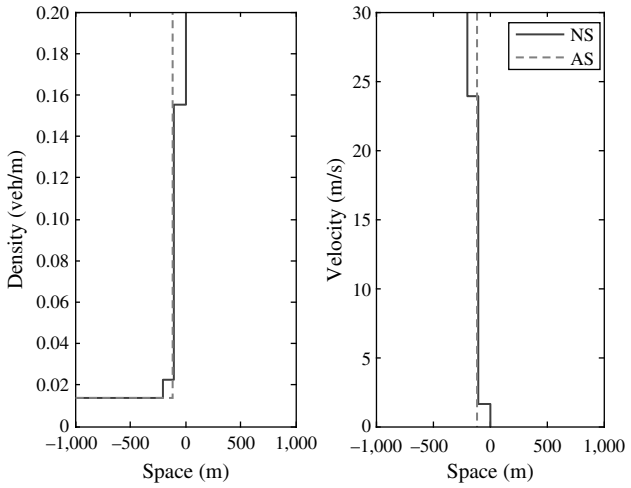

Figure 11 **Case 2.1.1: Analytical and Numerical Riemann Problem Solutions in (ρ, x) and (v, x) Coordinates ($\Delta x = 100$ m and $\Delta t = 2$ s)**

Note. Reimann test problem (AS: analytic solution; NS: numerical solution).

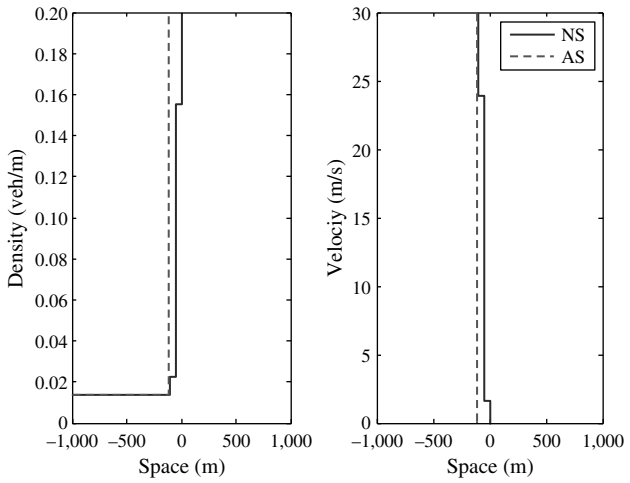

Figure 12 **Case 2.1.1: Analytical and Numerical Riemann Problem Solutions in (ρ, x) and (v, x) Coordinates ($\Delta x = 50$ m and $\Delta t = 1$ s)**

Note. Reimann test problem (AS: analytic solution; NS: numerical solution).

Case 2. $y = \rho(v - V_e(\rho)) < 0$. In this case, the fixed initial conditions are

$$U_l = (\rho_l = \rho_{cr}/2, v_l < V_e(\rho_{cr}/2)) \quad \text{and}$$
$$U_r = (\rho_r = \rho_{\max}/2, v_r < V_e(\rho_{\max}/2)).$$

The Riemann problem is identical to that in Case 1. Drawing both solutions, we can observe that the numerical solution is very close to the analytical solution. Figure 13 reports the time/space evolution of four traffic variables: density, speed, relative flow, and deduced relative speed (I), defined as $I = y/\rho = v - V_e(\rho)$ at time $t = 40$ seconds. Moreover, the decrease of the space and time discretisation time slice indicates a better convergence of the numerical solution towards the analytical one.

Case 3. $y = \rho(v - V_e(\rho)) > 0$. This case corresponds to Case 2.2 of the Riemann problem. We have chosen to test here the numerical approximation of a case involving a rarefaction wave. The initial conditions are defined as: upstream traffic state $U_l = (\rho_l = \rho_{\max}/2, v_l = (y_l/\rho_l) + V_e(\rho_l))$ and downstream traffic state $U_r = (\rho_r = \rho_{cr}/4, v_r = (y_l/\rho_l) + V_e(\rho_{cr}/2))$. Drawing both solutions (see Figure 15), we demonstrate again that both solutions are very similar to each other. The solutions are depicted at time $t =$ 40 seconds.

Again, if the time slice is decreased, the numerical solution is improved with respect to the analytical solution.

Considering that the CFL condition imposes relatively coarse space discretisation, some numerical viscosity is unavoidable, as can be observed in the preceding Figures 11 to 16.

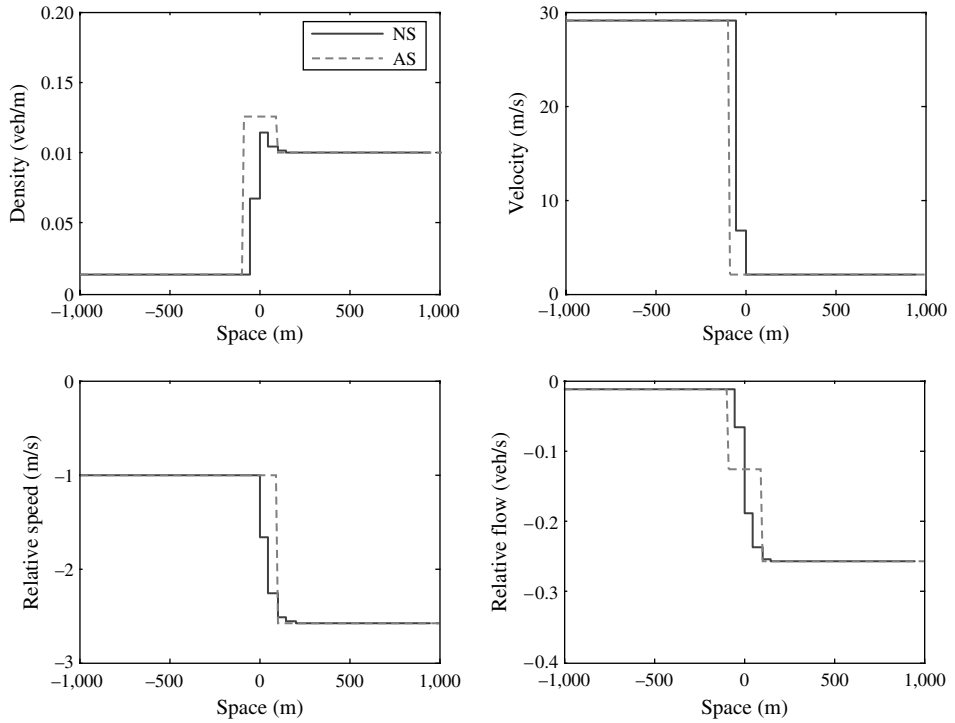

Figure 13 **Case 2.1.1: Analytical and Numerical Riemann Problem Solutions in** (ρ, x) **and** (v, x) **Coordinates (**$\Delta x = 100$ m **and** $\Delta t = 2$ s**)**
Note. Reimann test problem (AS: analytic solution; NS: numerical solution).

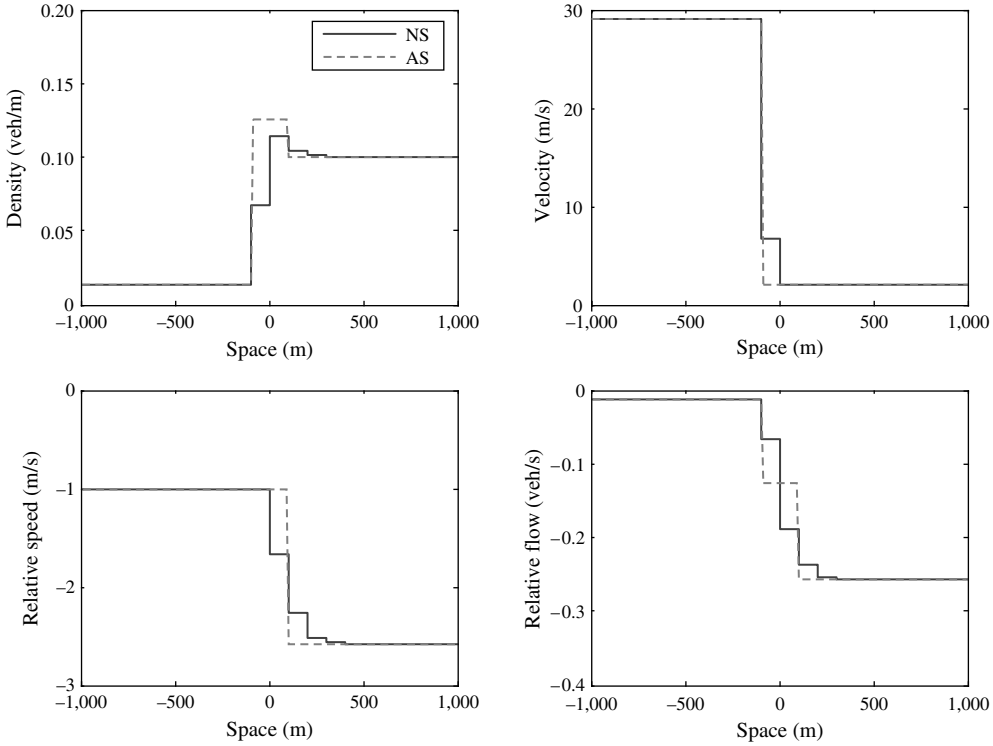

Figure 14 **Case 2.1.1: Analytical and Numerical Riemann Problem Solutions in** (ρ, x) **and** (v, x) **Coordinates (**$\Delta x = 50$ m **and** $\Delta t = 1$ s**)**
Note. Reimann test problem (AS: analytic solution; NS: numerical solution).

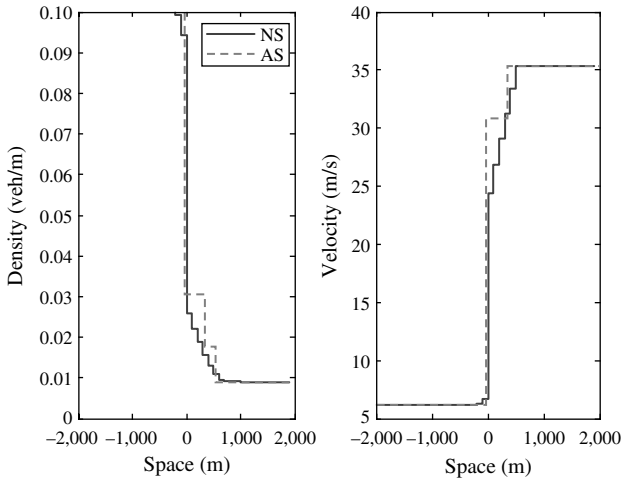

Figure 15 **Case 2.2: Analytical and Numerical Riemann Problem Solutions in (ρ, x) and (v, x) Coordinates ($\Delta x = 100$ m and $\Delta t = 2$ s)**

Note. Reimann test problem (AS: analytic solution; NS: numerical solution).

6. Application of the ARZ Model on Real Site

To evaluate the ability of the model to reproduce real traffic and based on the analysis of the previous sections, the ARZ model is applied on a motorway real site (see Figure 17). The total length of the considered motorway test site is about 2,500 m, including five measurement stations of traffic volume, occupancy rate, and speed aggregated on one-minute time intervals. This part of the motorway is particularly congested during the morning peak period. For the simulation, the selected measurement set is about two hours. The motorway stretch is subdivided into five links: three links, one origin, and one destination.

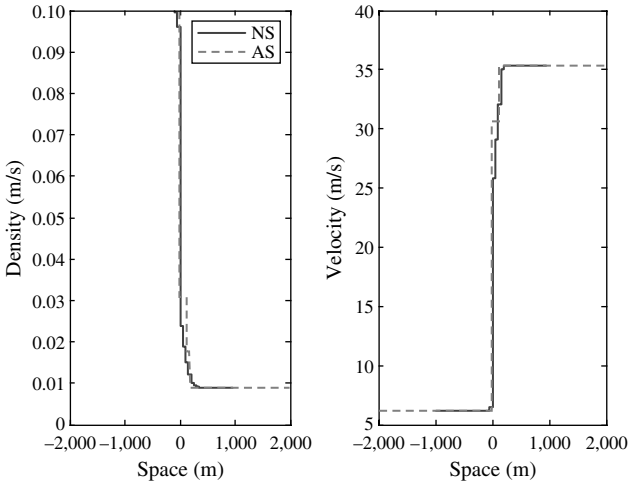

Figure 16 **Case 2.2: Analytical and Numerical Riemann Problem Solutions in (ρ, x) and (v, x) Coordinates ($\Delta x = 50$ m and $\Delta t = 1$ s)**

Note. Reimann test problem (AS: analytic solution; NS: numerical solution).

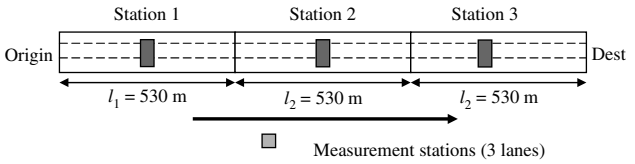

Figure 17 **Stretch of the Test Site**

Based on the real data measurements, the equilibrium fundamental diagram and its parameters are reported in Figure 18. In fact, the estimation procedure is not based on automatic calibration but it uses only uses EXCEL sheets and qualitative estimations are used, based on the physical characteristics of the motorway and current speed limitations. The outcome of this procedure gives $V_{\max} = 126$ km/hour, $\rho_{cr} = 35$ veh/km/lane, $V_{cr} = 65$ km/h, and maximum occupancy rate ($\mathrm{OCC}_{\max}$) = 58%.

The time interval of the simulation is equal to 10 seconds. The horizon of the simulation is limited to the morning peak period for 6 h–8 h, where traffic conditions evolve from fluid to congested, and vice-versa. Consequently, all cases of the Riemann problem are covered.

Boundary conditions at the origin are taken to be the inflow and the relative flow (the reader is referred to Lebacque, Mammar, and Haj-Salem (2007b) for a rigorous specification of boundary conditions in terms of local traffic supply and demand). The relative flow is estimated when the fundamental diagram parameters have been estimated. At the destination outflow is given; relative flow always propagates at the speed of traffic and, therefore, does not need to be specified at the destination.

Figure 19(a)–(d) depicts the time evolution of the four traffic variables: traffic volume, density, speed, and relative speed of measured and simulated data, respectively. Despite the simplicity of the calibration procedure of the equilibrium relationship of the fundamental diagram, the trajectories of the four simulated variables cope with the measurements with an

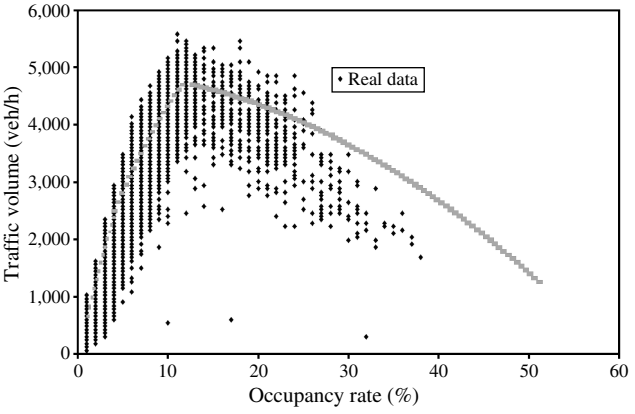

Figure 18 **Fundamental Diagram Parameters Estimation**

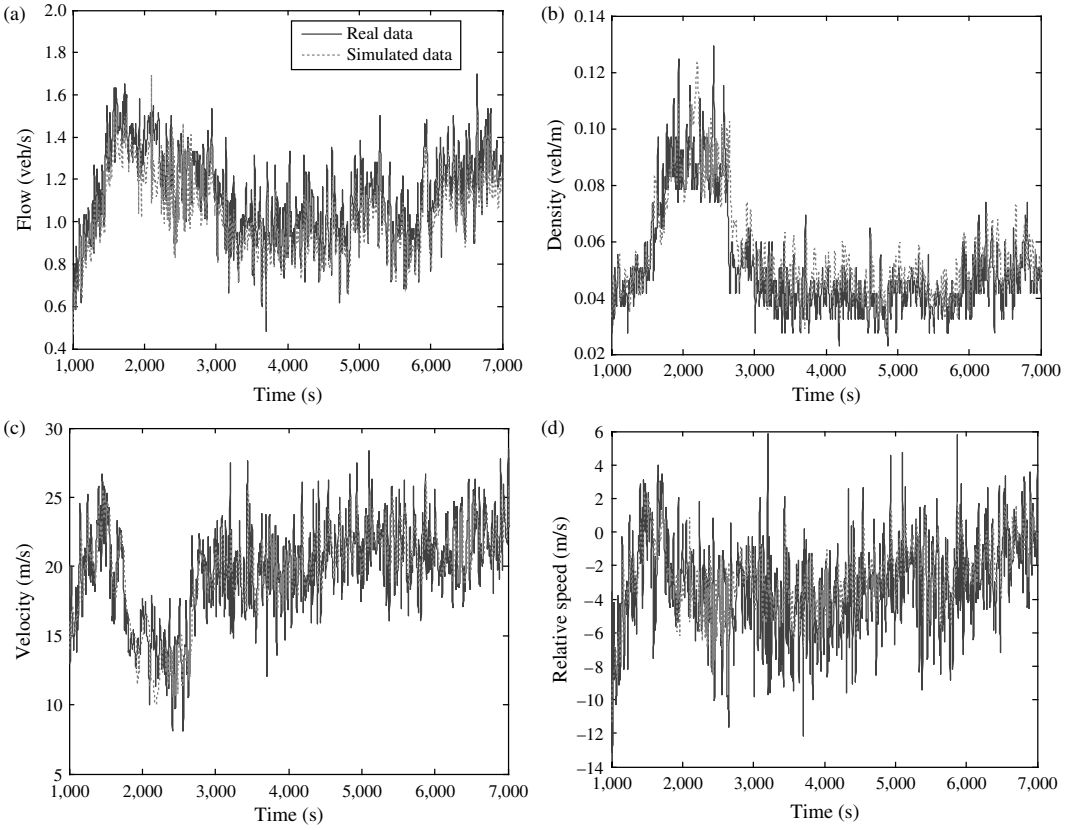

Figure 19 **Time Evolution of the Traffic Volume, Density, Speed, and Relative Speed (Measured and Simulated by the ARZ Model) Station2**

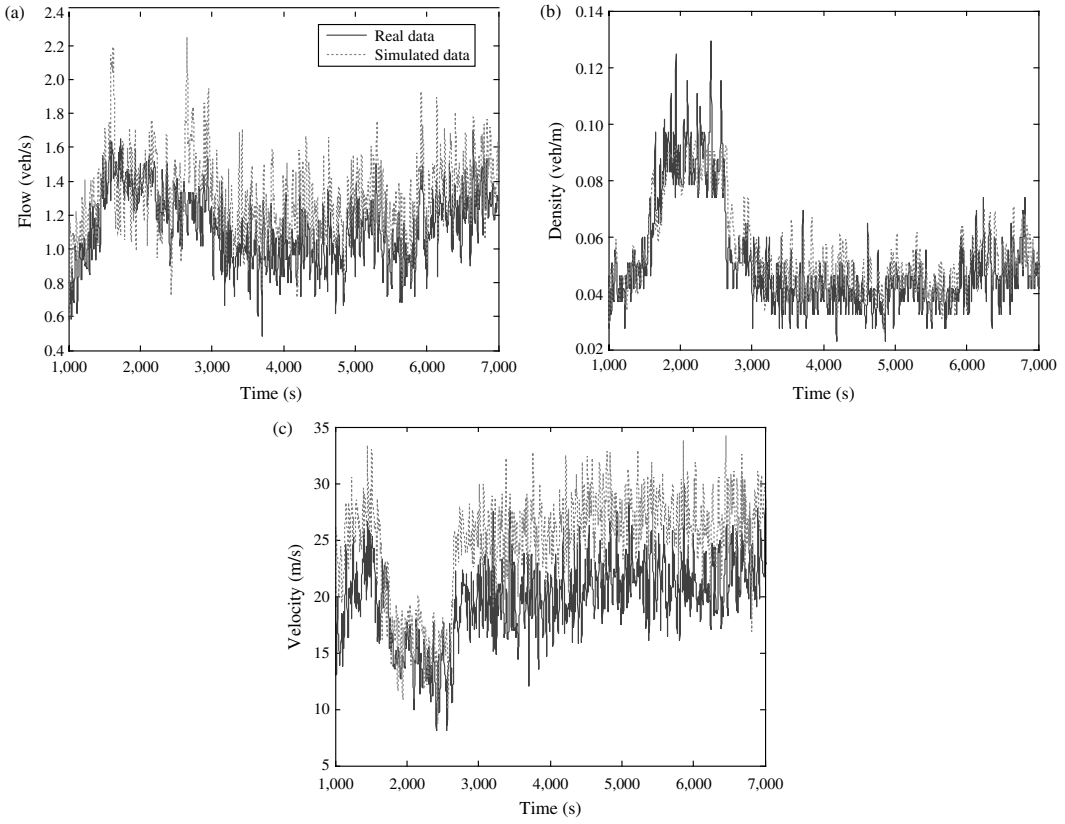

Figure 20 **LWR: Time Evolution of the Traffic Volume, Density, and Speed (Measured and Simulated by the LWR Model) Station2**

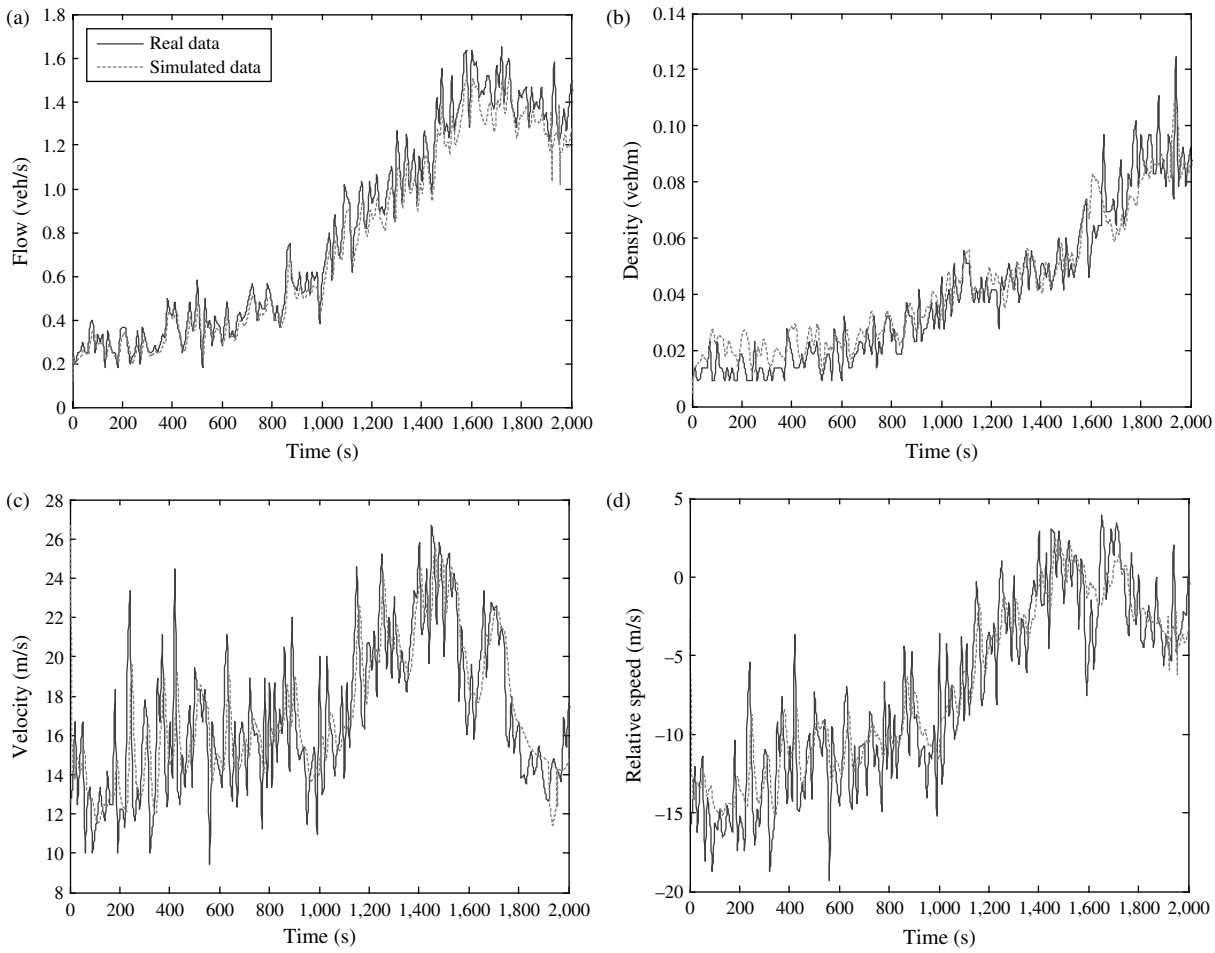

Figure 21 **Time Evolution of the Traffic Volume, Density, Speed, and Relative Speed (Measured and Simulated by the ARZ Model) Station2, Expanded Time Scale**

acceptable accuracy. The congestion is reproduced at the same time and space as the measurements.

To check the added value of the second-order ARZ model and using the fact that the LWR is embedded in the ARZ model (i.e., LWR = ARZ with zero relative speed), the estimated relative speed profile ($I(t)$), based on real data measurements and the equilibrium fundamental diagram, is set equal to 0. This means that the speed is equal to the equilibrium speed $V_e(\rho)$, both at the boundary and for initial data. In this case, the Equation (3) is dropped, and the model is equivalent to the first-order model (LWR):

$$\partial_t \rho + \partial_x(\rho V_e(\rho)) = 0, \quad \text{with } Q_e(\rho) = \rho V_e(\rho). \qquad (38)$$

The resolution of Equation (38) yields the solutions of the first-order modelling approach. Figure 20(a)–(c) represents the time and space evolution of traffic flow, density, and speed, respectively. Compared to the output results of the ARZ model (see Figure 19), the errors of LWR model with respect to the three traffic variables are higher.

Figures 21 and 22 depict the same results at an expanded scale (first half hour of the morning peak), emphasizing the differences between the two models. Figure 23 shows the systematic bias of the LWR model, which overestimates travel time and speed because it does not take into account relative speed.

These preliminary results indicate that the reconstruction of the traffic phenomenon, using a second-order model, is more accurate, compared to that of the first-order models.

If Z denotes a traffic variable, the corresponding mean square error is given by

$$\text{MSE} = \frac{1}{N}\sqrt{\sum_N (Z_{\text{measures}} - Z_{\text{model}})^2}.$$

The following table shows the MSE for the three fundamental traffic variables:

	Traffic variables		
Model	Flow (veh/h)	Density (veh/km)	Velocity (km/h)
ARZ model	113.76	516	2.76
LWR model	121.89	518	4.03

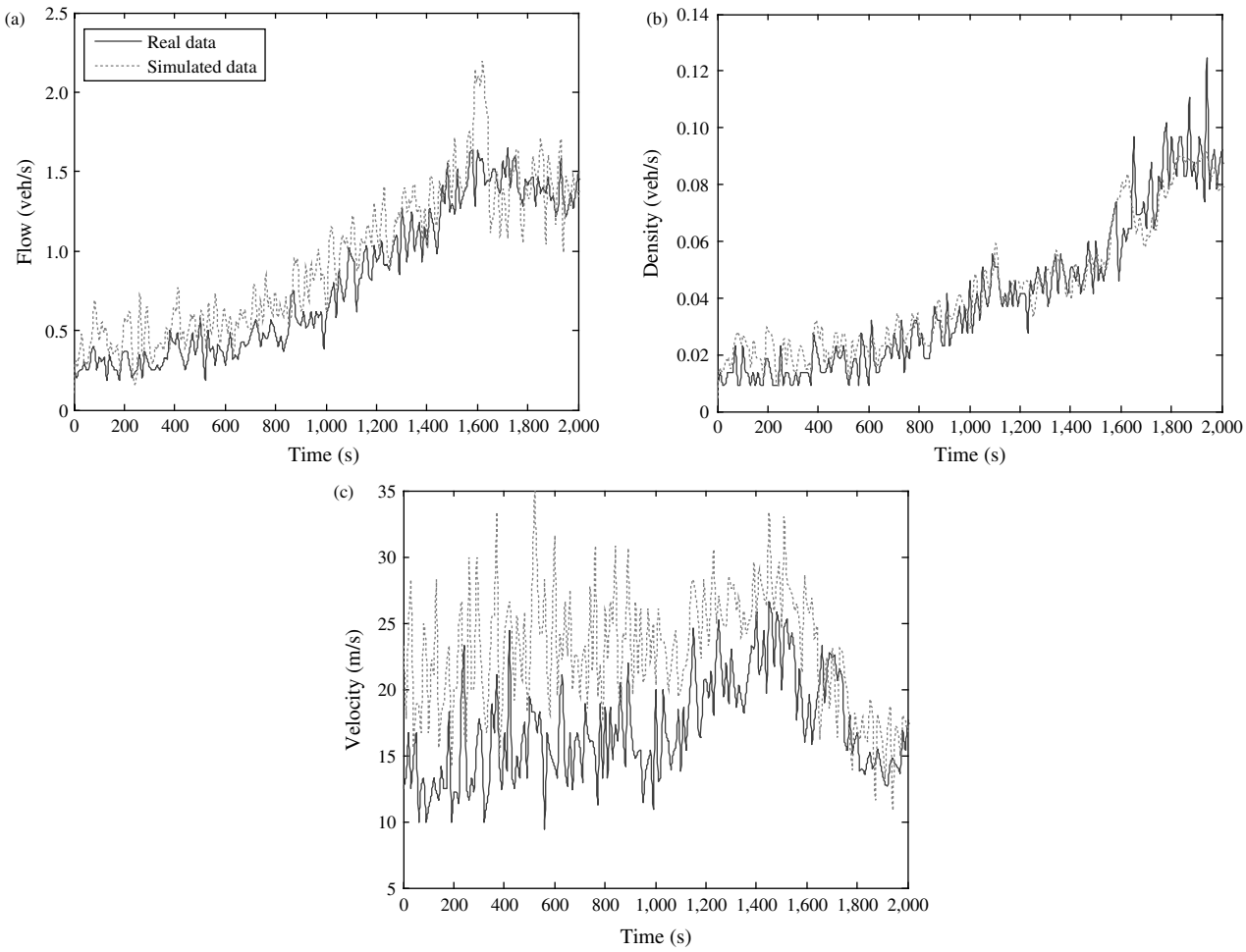

Figure 22 **Time Evolution of Traffic Volume, Density, Speed (Measured and Simulated by the LWR Model) Station2, Expanded Time Scale**

Figure 24 illustrates the time evolution of the traffic error flow and speed and shows in detail that the ARZ model outperforms the LWR model with the chosen set of fundamental diagram parameters.

Let us recall that the parameters of the fundamental diagram were estimated mainly on the basis of physical a priori estimates (jam density, desired speed, maximum flow, etc). The reason that the ARZ model performs better than the LWR model is that the ARZ model is endowed with a supplementary degree of liberty: the relative flow, which is estimated at the entrance of the system and then is propagated. The good fit of the ARZ model with measurements also suggests that the relative flow is indeed propagated in a fashion that is close to that implied by the momentum in Equation (2).

7. Conclusions

The extension of the fundamental diagram introduced in Lebacque et al. (2007a) makes it possible to solve the Riemann problem in the homogeneous case for all initial data and to obtain solutions that are physical in the following sense: speeds are positive, and density is positive and less than maximum density.

Ongoing research and future work concerning the ARZ model include analysis of the inhomogeneous

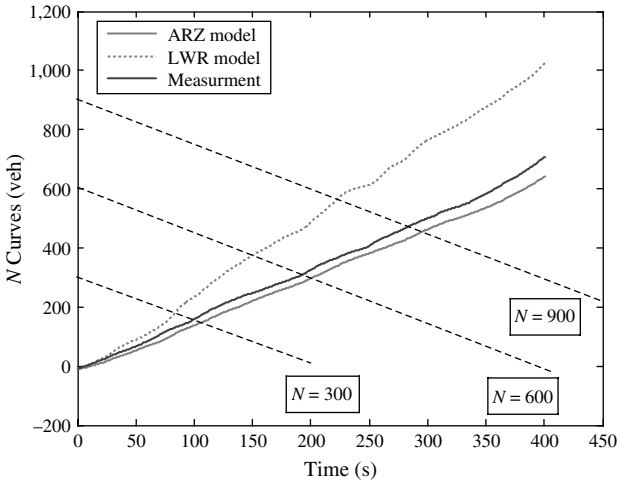

Figure 23 ***N*-Curves (Cumulative Flows at Station 2) (Measured vs. Simulated by the ARZ and the LWR Models), Expanded Time Scale**

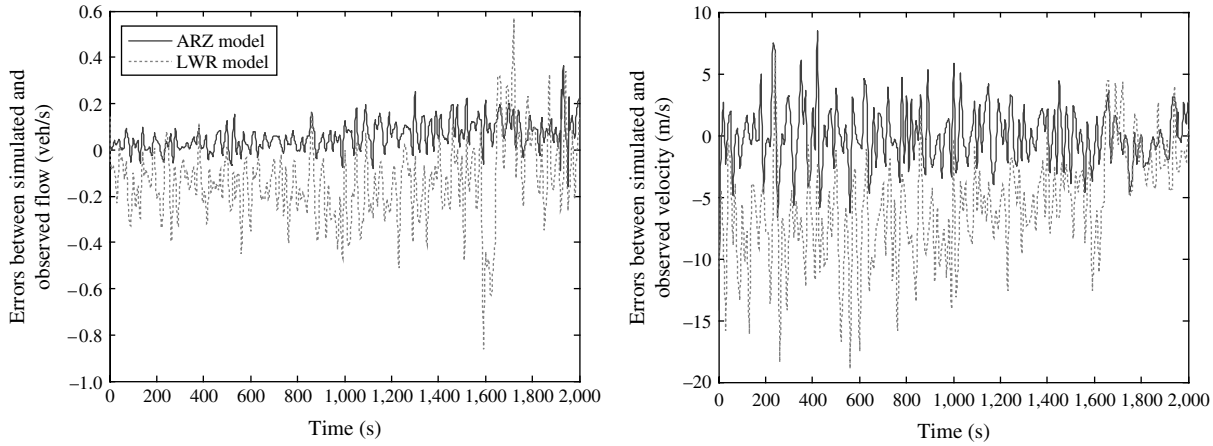

Figure 24 Time Evolution of Traffic Error Flow and Speed

Riemann problem (Lebacque et al.), development of the Godunov scheme for network modeling, and inclusion of the relaxation term into the solution scheme. The calibration and the validation process will also be investigated.

Acknowledgments

The authors gratefully acknowledge the support of the ACI-NIM (Action Concertée Imitative) NIM (Nouvelles Interfaces des Mathématiques) "Modélisation mathématique du trafic automobile" of the French Ministry for Higher Education and Research. The first author gratefully acknowledges the support of the "CIFRE" convention between INRETS, PHOENIX, and Université Val-d'Essonne.

References

Aw, A., M. Rascle. 2000. Resurrection of second order models of traffic flow. *SIAM J. Appl. Math.* **60**(3) 916–938.

Daganzo, C. F. 1995. Requiem for second-order fluid approximations of traffic flow. *Transportation Res. B* **29** 277–286.

Del Castillo, J.-M., P. Pintado, F. G. Benitz. 1993. A formulation of reaction time of traffic flow models. C. F. Daganzo, ed. *Proc. 12th Internat. Sympos. Transportation Traffic Flow Theory*. Elsevier, Amsterdam, 387–405.

Jiang, R., Q. S. Wu, Z. J. Zhu. 2002. A new continuum model for traffic flow and numerical tests. *Transportation Res. Part B* **36**(5) 405–419.

Kröner, D. 1997. *Numerical Schemes for Conservation Laws*. Wiley Teubner, New York.

Lebacque, J. P. 1996. The Godunov scheme and what it means for first order traffic flow models. *Transportation and Traffic Theory, Proc. 13th Internat. Sympos. Transportation*. Elsevier, Amsterdam, 647–677.

Lebacque, J. P., S. Mammar, H. Haj-Salem. 2007a. The Aw-Rascle-Zhang model: Vacuum problems, existence and regularity of the solutions of the Riemann problem. *Transportation Res. Part B* **41**(7) 710–721.

Lebacque, J. P., S. Mammar, H. Haj-Salem. 2007b. Generic second order traffic flow modelling. *Proc. 17th Internat. Sympos. Transportation Traffic Theory*. Elsevier, Amsterdam, 755–766.

Lighthill, M. H., G. B. Whitham. 1955. On kinematic waves II: A theory of traffic flow on long crowded roads. *Proc. Roy. Soc. (Lond.) A* **229** 317–345.

Payne, H. J. 1971. Models of freeway traffic and control. *Simulation Councils Proc. Ser. Math. Models Public Syst.* **28**(1) 51–61.

Ross, P. 1988. Traffic dynamics. *Transportation Res. Part B* **22**(6) 421–435.

Richards, P. I. 1956. Shock-waves on the highway. *Oper. Res.* **4** 42–51.

Zhang, H. M. 1998. A theory of nonequilibrium traffic flow. *Transportation Res. Part B* **32** 485–498.

Witham, G. B. *Linear and Nonlinear Waves*. Wiley, New York.

Zhang, H. M. 2002. A non-equilibrium traffic model devoid of gas-like behavior. *Transportation Res. Part B* **36** 275–290.